

# Accurate and realistic initial data for black hole-neutron star binaries.

Philippe Grandclément\*

*Laboratoire de l'Univers et de ses Théories, UMR 8102 du C.N.R.S.,  
Observatoire de Paris, F-92195 Meudon Cedex, France*

(Dated: December 2, 2024)

This paper is devoted to the computation of compact binaries composed of one black hole and one neutron star. The objects are assumed to be on exact circular orbits. Standard 3+1 decomposition of Einstein equations is performed and the conformal flatness approximation is used. The obtained system of elliptic equations is solved by means of multi-domain spectral methods. Results are compared with previous work both in the high mass ratio limit and for one neutron star with very low compactness parameter. The accuracy of the present code is shown to be greater than with previous codes. Moreover, for the first time, some sequences containing one neutron star of realistic compactness are presented and discussed.

PACS numbers: 04.25.Dm,04.30.Db,04.40.Dg

## INTRODUCTION

Motivated by the various gravitational wave detectors coming online [1, 2], numerical simulations of binary compact objects have been greatly investigated in the last years. With the progress made for the evolution of both binary neutron stars (BNS) [3] and binary black holes (BBH) [4, 5, 6], it seems timely to turn to the last interesting type of binary, a system composed of one black hole and one neutron star (BHNS). The evolution synthesis codes indicate that the detection rate of BHNS with LIGO/Virgo will be as high (if not higher) than the one for BNS systems (see Table 6 of [7]). Simulations of coalescing binary systems usually proceeds in two steps. First one needs to produce initial data that verify Einstein constrain equations and that are as physically relevant as possible. Then those initial configurations are evolved forward in time. Those steps involve rather different techniques and are equally challenging.

Most of the initial data for coalescing binaries rely on the quasiequilibrium hypothesis that assumes that the objects are on exact closed circular orbits. This is of course only an approximation, no closed orbits existing in general relativity for such systems. However, for sufficiently large separations, this should be close to reality. The quasiequilibrium approximation has been applied to BBH and BNS systems (see for example [8, 9, 10, 11]) and the obtained initial data have been successfully evolved, indeed exhibiting circular-like trajectories [3, 4, 5, 6]. The aim of this paper is to apply the same technique to a BHNS, without assuming extreme mass ratios like in [12]. On the contrary, a moderate mass ratio of 5 is used. This value is chosen mainly for comparisons with previous work [13] but is sufficient to demonstrate the ability of the code to handle binaries with close masses. Let us mention that the simulations of the formation of compact binaries indicate a slightly lower mass ratio to be more probable [14]. The present work shares some properties with [13] even if some details are different. Moreover, one of the main shortcomings of [13] is the fact that it consider a NS of unrealistic compactness, as small as 0.0879. This implies a mass close to  $0.7 M_\odot$  for most of the available EOS, which is much smaller than the canonical value of  $1.2 - 1.4 M_\odot$ . On the contrary, in this work and for the first time, a BHNS with a realistic NS is computed. Indeed, the most compact star presented here has a compactness of 0.15 which makes its mass in the range  $1.2 - 1.5 M_\odot$  depending on the EOS.

## EQUATIONS

The standard 3+1 decomposition of Einstein equations is used, in which the spacetime is foliated by a family of spatial hypersurfaces. The 4-dimensional metric is given in terms of the lapse function  $N$ , the shift vector  $\beta^i$  and the spatial metric  $\gamma_{ij}$ . The evolution of the spatial metric is described by the second fundamental form: the extrinsic curvature tensor  $K_{ij}$  which is the Lie derivative of  $\gamma_{ij}$  along the normal to the hypersurfaces.

The conformal factor  $\Psi$  is defined by  $\gamma_{ij} = \Psi^4 \tilde{\gamma}_{ij}$  and by demanding that the determinant of the conformal metric  $\tilde{\gamma}_{ij}$  is 1 (so that the determinant of  $\gamma_{ij}$  is  $\Psi^{12}$ ). A similar conformal decomposition is also performed on the extrinsic curvature tensor.

Before solving the constraint equations, there are some quantities that must be chosen. Those are the so-called “freely specifiable” variables. By this, one means that a solution of the constraint equations can be found for every choice of those variables. In the standard “thin-sandwich” approach, those variables are: the trace of the extrinsic

curvature  $K$  and its time derivative  $\partial_t K$ , the conformal metric  $\tilde{\gamma}_{ij}$  and its time derivative  $\tilde{u}_{ij} = \partial_t \tilde{\gamma}_{ij}$ . By working in the corotating frame, the quasiequilibrium approximation amounts to neglecting the variations with time for all the quantities. In particular, one will set  $\partial_t K = 0$  and  $\tilde{u}_{ij} = 0$ . Maximum slicing  $K = 0$  and conformal flatness  $\tilde{\gamma}_{ij} = f_{ij}$ ,  $f_{ij}$  being the 3-dimensional flat metric are also assumed. Even if the spatial metric for a binary system can not be flat, this approximation has proven to be more accurate than one could expect for both BBH and BNS [15, 16, 17]. Let us note that the choices for  $K$  and  $\tilde{\gamma}_{ij}$  are different from the ones made in [13] where the authors used values derived from the Kerr-Schild metric.

The mathematical problem is then to solve the following set of five elliptic coupled equations for the two scalars  $\Psi$  and  $N$  and the vector field  $\beta^i$  :

$$\Delta N = 4\pi N \Psi^4 (E + S) + N \Psi^4 \tilde{A}_{ij} \tilde{A}^{ij} - 2\bar{D}_i \ln \Psi \bar{D}^i N \quad (1)$$

$$\Delta \Psi = -2\pi \Psi^5 E - \frac{\Psi^5}{8} \tilde{A}_{ij} \tilde{A}^{ij} \quad (2)$$

$$\Delta \beta^i + \frac{1}{3} \bar{D}^i \bar{D}_j \beta^j = 16\pi N \Psi^4 (E + p) U^i + 2\tilde{A}^{ij} (\bar{D}_j N - 6N \bar{D}_j \ln \Psi) \quad (3)$$

where all the operators are associated with the flat metric. The conformal extrinsic curvature tensor  $\tilde{A}^{ij} = \Psi^4 K^{ij}$  relates to the lapse and shift vector by  $\tilde{A}^{ij} = 1/2N (\bar{D}^i \beta^j + \bar{D}^j \beta^i - 2/3 \bar{D}_k \beta^k f^{ij})$ . The quantities  $E$ ,  $S$ ,  $p$  and  $U^i$  are matter terms describing the NS fluid. In this paper, a polytropic equation of state relates the pressure to the fluid baryon number density by  $p = \kappa n^\Gamma$ . In all the following  $\Gamma$  is fixed to 2 and  $\kappa$  is varied to construct NS with various compactness. The star is also assumed to be irrotational so that the fluid dynamic is given by an elliptic equation for the potential of the flow.

The black hole is described by imposing apparent horizon boundaries on a sphere (see [18] for a detailed review on such conditions). This idea has been used successfully in the BBH field (see [11] for the last application to date). However, in this work, like in [9, 10], the lapse is set to 0 on the horizon. Doing so one needs to do small correction on the shift vector to get a regular extrinsic curvature tensor on the horizon. In the case of the BBH it has been shown that this correction was small enough [10]. In the BHNS case, the effect of the neutron star on the horizon is even smaller, making this relative correction very small ( $\lesssim 2 \cdot 10^{-4}$  for our innermost configurations). An important difference with respect to what was done in [10], concerns the rotation state of the black hole. Indeed, it seems unlikely that it will be synchronized with the orbital motion and one will instead consider an irrotational black hole. Like in Sec. VB of [11], a local rotation rate is imposed to ensure that the local angular momentum vanishes. This is to be contrasted with what is done in [13] where the authors imposed irrotationality only to the first order (see Sec. VA of [11]).

Standard asymptotical flatness is imposed to get appropriate boundary conditions at infinity.

## NUMERICS, TESTS AND COMPARISONS

The system (1-3) is solved using the LORENE library [19]. This library is developed mainly at the Meudon site of Paris observatory and has been successfully apply to the computation of various problems in general relativity (see references at [19]). The basic features of Lorene are the following. Spectral methods in spherical coordinates are employed, mainly using spherical harmonics or trigonometrical functions for the angles  $(\theta, \varphi)$  and Chebyshev polynomials for the radial coordinate  $r$ . Space is decomposed in various spherical-like shells, the spectral expansion being done in each of those domains. Space is compactified by means of the variable  $u = 1/r$  in the outermost domain. This enables to impose exact boundary conditions at infinity, the computational domain covering the whole space. Two sets of such domains are used, one centered around each compact object and the equations (1-3) are split on those two sets of domains (see for example [8] and [10] for explicit implementations of this method). For the NS, the first domain is adapted to match the surface of the star, thus getting rid of any Gibbs phenomenon that would be caused by some discontinuities at the surface. With such methods, solving elliptic equations amounts to inverting some matrices. Explicit examples are given in [20]. Let us mention that the code of [13] is also based the LORENE library. However the two codes have been written completely independently and the details of the two implementations are not the same. As will be seen, it turns out that the performance of the two codes are rather different.

The system (1-3) is solved by iteration, until the fields converge to a given threshold (typically  $10^{-7}$ ). During the course of the iteration, various quantities are changed in order to fulfill various requirements. For example, the central enthalpy of the NS is rescaled at each step in order to get a neutron star of given baryon mass (see Sec. IVD3 of [8]).

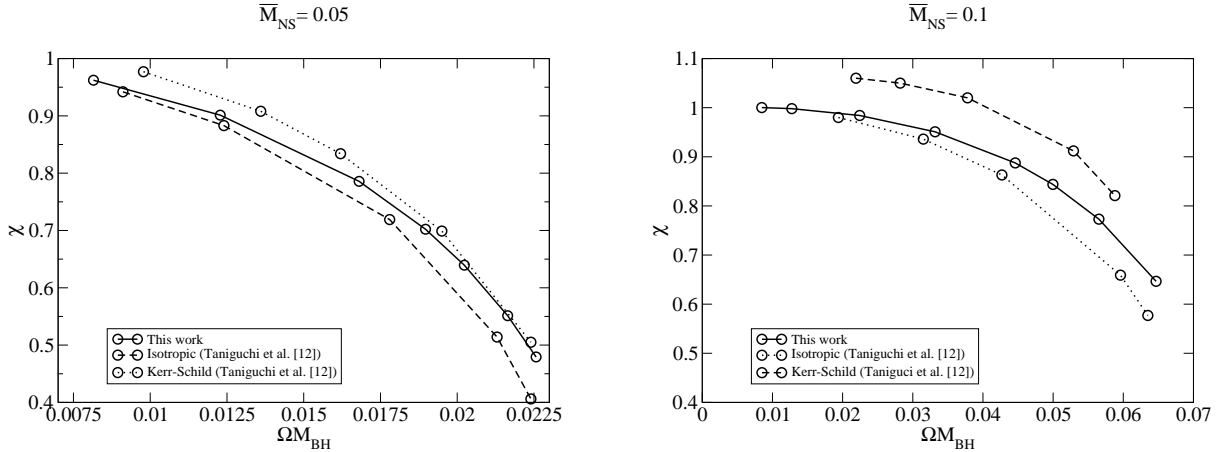


FIG. 1: Deformation indicator  $\chi$  as a function of the orbital frequency, for various approaches and  $\bar{M}_{\text{NS}} = 0.05$  (first panel) and  $\bar{M}_{\text{NS}} = 0.1$  (second panel). The mass ratio is 10.

The same technique is also used to modify: the radius of the black hole to get a given irreducible mass, the position of the rotation axis to ensure that the total linear momentum vanishes, the local rotation rate of the black hole to impose irrotationality. The distance between the two objects can also be modified by this means. Like in [8], the orbital velocity is determined so that the gradient of enthalpy of the fluid lies at the origin of the grid of the NS.

For both objects, space is decomposed on typically 8 or 9 domains, each of them being covered by  $N_r \times N_\theta \times N_\varphi = 33 \times 21 \times 20$  points. The achieved precision can be asserted by some global checks. For instance, if Eq. (2) is fulfilled, the ADM mass can be computed in two ways: either by the standard integral at infinity, or by a volume integral plus an integral on the BH horizon (see Sec. IIID of [8]). For all our configurations, the relative difference between the two values is less than a few  $10^{-5}$ . Other criteria of this kind can be derived that test the other equations (using the total angular momentum  $J$  and the generalized Smarr formula ; see Sec. IIIC and IIID of [9]). However, in those cases, the precision is also limited by the regularization of the shift on the horizon but the error is at most of the order of  $10^{-2}$  for the innermost configurations.

Another test is provided by comparing the results from this work with the ones obtained in the extreme mass ratio in [12]. More precisely, on Fig. 1, one shows the value of  $\chi$  as a function of the orbital frequency, for a mass ratio  $M_{\text{BH}}^{\text{irr}}/M_{\text{NS}}^{\text{b}} = 10$ .  $M_{\text{BH}}^{\text{irr}}$  denotes the irreducible mass of the BH and  $M_{\text{NS}}^{\text{b}}$  the baryonic mass of the NS, both quantities being kept constant along a sequence.  $\chi$  is a measure of the deformation of the star. It is 1 for a spherical star and 0 at the mass-shedding limit (see Eq. (52) of [12] for the precise definition). The first panel of Fig. 1 shows the value of  $\chi$  for  $\bar{M}_{\text{NS}}^{\text{b}} = 0.05$  and the second one for  $\bar{M}_{\text{NS}}^{\text{b}} = 0.1$ , the masses being expressed in standard polytropic units. The agreement with [12] is good, especially for the isotropic background. The difference is more important with the Kerr-Schild approach but one can note that those results look rather unphysical,  $\chi$  being even greater than 1 for some values of  $\Omega M_{\text{BH}}$  and  $\bar{M}_{\text{NS}} = 0.1$ .

Another comparison can be made with the sequence presented in [13], that relies on an approach similar to the work presented here. Let us first mention that the “neutron star” presented in [13] is highly non-realistic, having a compactness as small as  $\Xi = 0.0879$ . One can only wonder why such low value has been chosen. Anyway, for comparison purposes, a sequence with the same parameters has been computed with the code described here. On the first panel of Fig. 2 the value of  $\chi$  as a function of  $\Omega M_0$  is shown. In all the following,  $M_0$  denotes the total gravitational mass for infinite separation, that is the sum of the BH irreducible mass  $M_{\text{BH}}^{\text{irr}}$  and the gravitational mass (i.e. the ADM mass) of the isolated NS:  $M_{\text{NS}}^{\text{grav}0}$ . One of the most striking feature of the first panel is that the data from [13] are extremely noisy. It is highly unlikely that this comes solely from the use of the Kerr-Schild approach. It seems that the code from [13] can not handle properly configurations with large to moderate separations, probably due to a purely numerical effect. On the contrary, the curve from this work exhibits a very smooth and satisfactory behavior. Anyway, the two curves agree reasonably well for large values of  $\Omega M_0$ , that is for small separations. The second panel of Fig. 2 shows the binding energy of the binary defined as  $E_b = M_{\text{ADM}}/M_0 - 1$ , as a function of  $\Omega M_0$ . The results from the two approaches differ quite a lot, the configurations from [13] being more bounded by a factor of 3. For comparison, the binding energy from both Newtonian and 3.5 PN theories are shown (given by Eq. (194) of [21]). The PN result is clearly much closer to the result of this paper. This closeness is a strong indication that

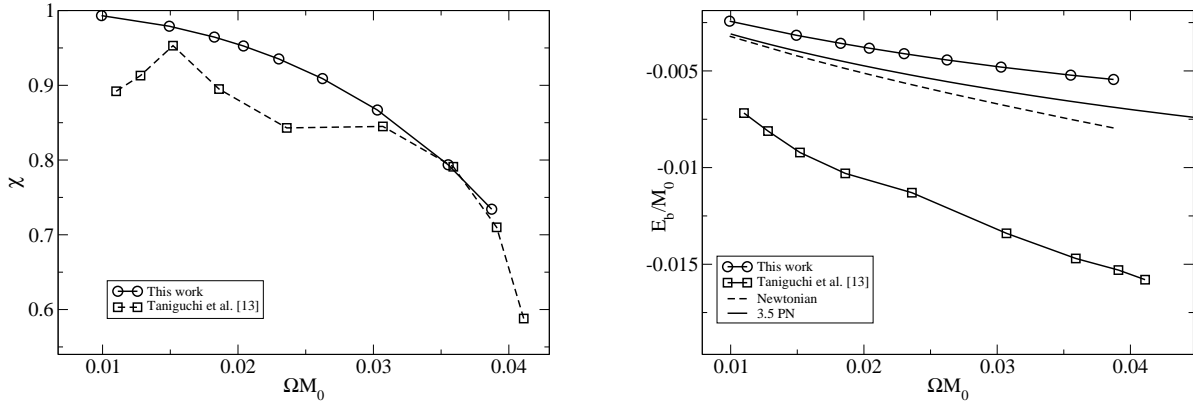


FIG. 2: Comparison between this work and [13] for a NS of small compactness ( $\Xi = 0.0879$ ). The ratio between the BH mass and the NS mass is 5. The first panel shows the deformation parameter  $\chi$  and the second one the binding energy, both as a function of the orbital velocity.

the conformal flatness approximation is rather good because PN expansion does not make us of it. The disagreement with [13] could come from the differences in the choices of the “freely-specifiable” variables. If this is the case, the difference between their results and the PN ones seems to indicate that the Kerr-Schild approach is not a valuable one. However, it may be that this disagreement comes from another effect. We also compared the total angular momentum coming from the two approaches (not shown here). The agreement is rather good, the difference being only of the order of 4% which is also the order of the difference with the PN result.

### MORE REALISTIC NEUTRON STARS

As already stated, the NS presented in the previous section has a very small compactness. In order to get more realistic neutron stars, one wishes to increase this parameter. This is done easily by decreasing the parameter  $\kappa$  in the EOS. The baryon mass of the NS is set so that they all have the same gravitational mass when isolated, i.e. the same  $M_{\text{NS}}^{\text{grav}0}$ . Doing so, BHNS with four different compactness parameters (0.075, 0.100, 0.125 and 0.150) are constructed. As in the previous section the ratio  $M_{\text{BH}}^{\text{irr}}/M_{\text{NS}}^{\text{grav}0}$  is set to 5.

The first panel of Fig. 3 shows the deformation  $\chi$  as a function of  $\Omega M_0$ . As can be expected, the more compact stars are less easily deformed and can survive closer to the black hole without being tidally destroyed. The second panel shows the binding energy of the binaries, along with the 3.5 PN result for point masses. The more compact configurations have smaller binding energy, which is an effect already observed for irrotational BNS (see for instance [22]). Once again, the more compact the NS and the closer it can get to the BH. It turns out that for the most compact star, the binding energy attains a minimum before the NS is destroyed. This means that the system can reach dynamical instability. This is also marginally the case for a compactness of 0.125. The two less compact stars, however, are destroyed before reaching the dynamical instability. This explains why all the configurations of [13] are found to be stable: the compactness of the star is small enough that it is destroyed before reaching the innermost stable orbit. The nature of the end point of a sequence thus depend on the compactness of the star and this is an effect that could have some implication on the emitted gravitational signal.

The total angular momentum  $J$  can also be computed. When it admits a minimum (i.e. for the two most compact stars), its position in terms of frequency is consistent with the one for the binding energy (even if they do not coincide exactly). The relative importance of the BH local rotation can also be investigated by computing the ratio  $f_r$  (see Sec. VB of [11]). It turns out that  $f_r$  is close to one (at most 0.91) which shows that the presence of the neutron star has a moderate influence on the structure of the BH horizon.  $f_r$  is almost independent of the compactness of the star. However its dependence with frequency is different from Eq. (58) of [11]. This is probably simply an effect of the mass ratio (5 in this work and 1 in [11]). Finally one turns to the viriel theorem which states that the Komar-like mass and ADM mass should be equal for circular orbits. Contrary to the case of BBH [9, 10, 11], this is not enforced exactly, the value of the orbital velocity being given by equilibrium of the NS fluid. However, the viriel can be used as a test

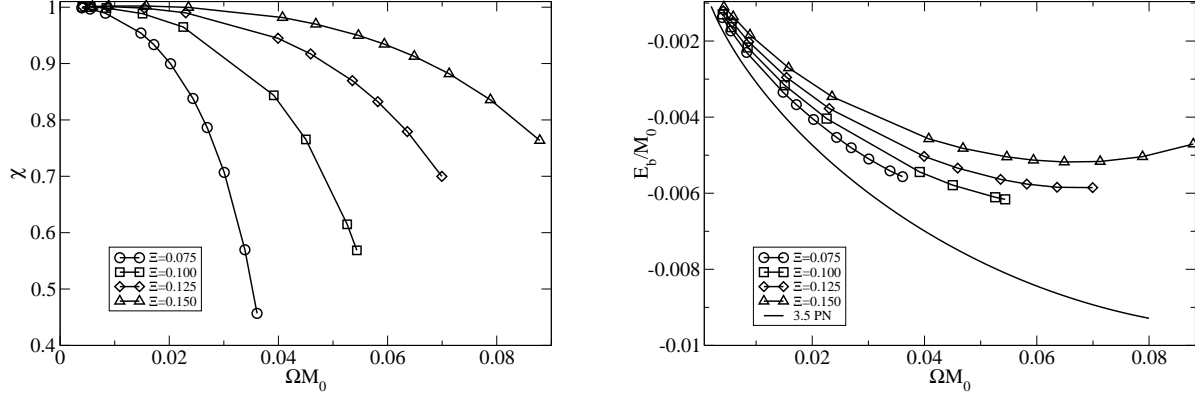


FIG. 3: Deformation parameter  $\chi$  (first panel) and binding energy (second panel) as a function of orbital velocity for four different compactness parameters  $\Xi$ .  $M_{\text{NS}}^{\text{grav}0}$  is the same for all the stars and the mass ratio with respect to the BH irreducible mass is 5.

of the code. It turns out that the viriel is verified to better than 2% for all configurations, the dependency with the compactness of the NS being moderate. The difference between the two masses is greater for tighter configurations. This behavior is similar to what is found in [13] even if the curves do not match, probably because of the different choice of “freely specifiable” variables. The viriel violation must be a measure on how the computed configurations differ from exact circularity. In a sense, it reflects the true nature of the movement: a slow inspiral.

All the configurations presented in this paper have been made public on the LORENE website [19].

---

\* Electronic address: philippe.grandclement@obspm.fr

- [1] LIGO website : <http://www.ligo.caltech.edu>
- [2] EGO-VIRGO website : <http://www.ego-gw.it>
- [3] M. Shibata and K. Taniguchi, *Phys. Rev. D* **73**, 064027 (2006).
- [4] F. Pretorius, *Class. Quant. Grav* **23**, S529 (2006).
- [5] J.G. Baker, J. Centrella, D.I. Choi, M. Koppitz and J. van Meter, *Phys. Rev. D* **73**, 104002 (2006).
- [6] M. Campanelli, C.O. Lousto, P. Marronetti and Y. Zlochower, *Phys. Rev. Lett.* **96**, 111101 (2006).
- [7] K. Belczynski, V. Kalogera and T. Bulik, *Astrophys. J.* **572**, 407 (2001).
- [8] E. Gourgoulhon, P. Grandclément, K. Taniguchi, J.-A. Marck and S. Bonazzola, *Phys. Rev. D* **63**, 064029 (2001).
- [9] E. Gourgoulhon, P. Grandclément and S. Bonazzola, *Phys. Rev. D* **65**, 044020 (2002).
- [10] P. Grandclément, E. Gourgoulhon and S. Bonazzola, *Phys. Rev. D* **65**, 044021 (2002).
- [11] M. Caudill, G.B. Cook, J.D. Grisby and H.P. Pfeiffer, submitted to *Phys Rev D*, preprint gr-qc/0605053.
- [12] K. Taniguchi, T.W. Baumgarte, J.A. Faber and S.L. Shapiro, *Phys. Rev. D* **72**, 044008 (2005).
- [13] K. Taniguchi, T.W. Baumgarte, J.A. Faber and S.L. Shapiro, *Phys. Rev. D* **74**, 041502(R) (2006).
- [14] T. Bulik, D. Gondek-Rosinska and K. Belczynski, *Mon. Not. Roy. Astron. Soc.* **352**, 1372 (2004).
- [15] T. Damour, E. Gourgoulhon and P. Grandclément, *Phys. Rev. D* **66**, 024007 (2002).
- [16] L. Blanchet, *Phys. Rev. D* **65**, 124009 (2002).
- [17] K. Uryu, F. Limousin, J.L. Friedman, E. Gourgoulhon and M. Shibata, submitted to *Phys. Rev. D*, preprint gr-qc/0511136.
- [18] E. Gourgoulhon and J.L. Jaramillo, *Physics Report* **423**, 159 (2006).
- [19] Lorene website : <http://www.lorene.obspm.fr>
- [20] P. Grandclément, S. Bonazzola, E. Gourgoulhon and J.-A. Marck, *J. Comput. Phys.* **170**, 231 (2001).
- [21] L. Blanchet, *Living Rev. Relativity* **9**, 4 (2006). URL : <http://www.livingreviews.org/lrr-2006-4>.
- [22] K. Taniguchi and E. Gourgoulhon, *Phys. Rev. D* **68**, 124025 (2003).